

000 ALPHA SAGE: STRUCTURE-AWARE ALPHA MINING 001 002 VIA GFLOWNETS FOR ROBUST EXPLORATION 003 004

005 **Anonymous authors**

006 Paper under double-blind review

009 ABSTRACT 010

011 The automated mining of predictive signals, or alphas, is a central challenge
012 in quantitative finance. While Reinforcement Learning (RL) has emerged as a
013 promising paradigm for generating formulaic alphas, existing frameworks are fun-
014 damentally hampered by a triad of interconnected issues. First, they suffer from
015 reward sparsity, where meaningful feedback is only available upon the comple-
016 tion of a full formula, leading to inefficient and unstable exploration. Second,
017 they rely on semantically inadequate sequential representations of mathematical
018 expressions, failing to capture the structure that determine an alpha’s behavior.
019 Third, the standard RL objective of maximizing expected returns inherently drives
020 policies towards a single optimal mode, directly contradicting the practical need
021 for a diverse portfolio of non-correlated alphas. To overcome these challenges,
022 we introduce **AlphaSAGE** (Structure-Aware Alpha Mining via Generative Flow
023 Networks for Robust Exploration), a novel framework is built upon three cor-
024 nerstone innovations: (1) a structure-aware encoder based on Relational Graph
025 Convolutional Network (RGCN); (2) a new framework with Generative Flow
026 Networks (GFlowNets); and (3) a dense, multi-faceted reward structure. Em-
027 pirical results demonstrate that AlphaSAGE outperforms existing baselines in
028 mining a more diverse, novel, and highly predictive portfolio of alphas, thereby
029 proposing a new paradigm for automated alpha mining. Our code is available at
030 <https://anonymous.4open.science/r/AlphaSAGE-3BA9>.
031

032 1 INTRODUCTION

033 The primary objective in quantitative trading is to identify and exploit market inefficiencies, a pur-
034 suit centered on the mining of “alphas”. These alphas are predictive signals, typically represented
035 as mathematical expressions, that aim to forecast asset returns and thus serve as the cornerstone of
036 systematic trading strategies.¹ Therefore, *alpha mining* (efficient construction of high-quality al-
037 phas) constitutes the core of quantitative research: high-quality alphas enable more accurate return
038 forecasting, improved risk-adjusted portfolio construction, and ultimately superior excess returns.
039

040 Traditionally, alpha mining has been a manual, hypothesis-driven process. Researchers propose
041 financial or economic hypotheses, translate them into candidate alphas, and validate their predictive
042 power through statistical tests or backtesting. While this pipeline has led to influential discoveries
043 such as value, momentum, and quality alphas [Kakushadze \(2016\)](#), it suffers from limited scalability
044 and strong reliance on human intuition. With the increasing complexity of financial markets, the
045 hypothesis-driven paradigm struggles to cope with vast, non-linear interactions in high-dimensional
046 data, making it increasingly challenging to uncover novel and uncorrelated signals.
047

048 Recent advances have motivated the shift towards automated alpha mining, where machine learning
049 algorithms systematically search through the enormous combinatorial space of possible formulas.
050 Early efforts often relied on Genetic Algorithm (GA) [Chen et al. \(2021\)](#); [Zhang et al. \(2020\)](#); [Cui et al. \(2021\)](#), which evolves candidate formulas using mutation and crossover operators. Despite pro-
051 ducing interpretable formulas, GA methods can be computationally inefficient and tend to converge
052 to local optimum if mutation rate is not carefully designed. More recently, Reinforcement Learning
053 (RL) [Yu et al. \(2023\)](#); [Zhu & Zhu \(2025\)](#); [Zhao et al. \(2024\)](#); [Xu et al. \(2024\)](#) has emerged as a

¹An example of alpha is shown in Figure 1.

powerful alternative, framing alpha construction as a sequential decision-making process in which an agent incrementally builds formulas. RL-based methods promise higher efficiency and scalability but also inherit several critical challenges, including reward sparsity, structural underrepresentation, and limited diversity in generated alphas.

The direct application of RL to alpha mining is generally fraught with significant obstacles that limit its efficacy. First, current methodologies often suffer from a severe “cold-start” problem, as the reward signal—typically based on an alpha’s Information Coefficient (IC)—is extremely sparse [Zhao et al. \(2025\)](#). Second, most existing approaches represent alpha expressions as simple sequences of tokens, often processed by sequential models such as LSTMs. Such representations fail to capture the logical and hierarchical structure inherent in formulas. Finally, the traditional RL, which is designed to maximize a singular reward function, tends to produce a relatively uniform path for alpha mining, lacking the diversity essential for constructing robust portfolios [Tang et al. \(2025\)](#).

To overcome these limitations, we propose **AlphaSAGE** (Structure-Aware Alpha Mining via Generative Flow Networks for Robust Exploration), a comprehensive framework designed to address the core problems of exploration, semantic understanding, and diversity in alpha mining. To evaluate the effectiveness of the model, we conducted extensive experiments based on real historical data from both the Chinese and U.S. stock markets. The experimental results demonstrate that the model outperforms existing models across different markets.

In summary, our contributions are as follows:

- We introduce **a structure-aware encoder** based on Relational Graph Convolutional Network (RGCN) [Schlichtkrull et al. \(2018\)](#) that operates on Abstract Syntax Tree (AST) representations of alphas to capture their semantic and compositional nature.
- We propose **a generative framework** using Generative Flow Networks (GFlowNets) [Bengio et al. \(2021\)](#); [Malkin et al. \(2022\)](#); [Bengio et al. \(2023\)](#) that learns to sample a diverse set of candidates, directly addressing the need for a varied alpha portfolio.
- We present **a dense, multi-faceted reward function** that combines terminal performance with intrinsic rewards for structural integrity and novelty to effectively guide the GFlowNet’s exploration.

2 BACKGROUND AND RELATED WORK

2.1 ALPHA MINING AND COMBINATION

In quantitative finance, an *alpha* is a deterministic transformation of historical market data into a signal that aims to forecast future returns. When expressed as a symbolic program (e.g., an abstract syntax tree), an alpha remains interpretable and auditable. Alpha quality is commonly summarized by correlation-based metrics (e.g., IC) computed between alpha outputs and subsequent returns.

Early discovery pipelines were manual and hypothesis-driven. More recent automation—most notably genetic algorithm (GA) [Chen et al. \(2021\)](#); [Zhang et al. \(2020\)](#); [Cui et al. \(2021\)](#) and reinforcement learning (RL) [Yu et al. \(2023\)](#); [Zhu & Zhu \(2025\)](#); [Zhao et al. \(2024\)](#); [Xu et al. \(2024\)](#)—expanded the search space but introduced three recurring challenges: sparse and delayed rewards, weak encoding of alpha structure, and mode collapse toward a few similar solutions. Because single alphas are typically unstable across time and markets, practitioners assemble a library of alphas and combine them into a portfolio-level signal. Simple linear combinations are prevalent in practice, yet high correlations among alphas can make coefficient estimates unreliable and reduce both robustness and interpretability.

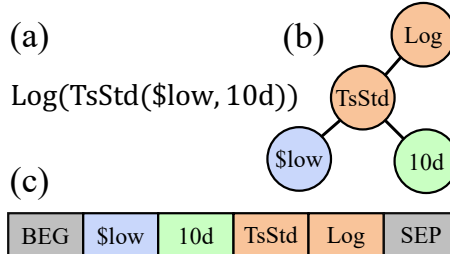


Figure 1: Different forms of alpha: (a) Formulated alpha; (b) Alpha’s expression tree; (c) Reverse Polish Notation (RPN) for alpha.

108 These observations motivate frameworks that jointly optimize for predictive power and diversity.
 109 Our design follows this principle: it encourages structurally distinct alphas during generation and
 110 combines them with a transparent, adaptively weighted scheme that emphasizes low cross-alpha
 111 dependence. Additional details appear in Appendix B.1.
 112

113 2.2 GRAPH NEURAL NETWORKS

114
 115 Graph neural networks (GNNs) Scarselli et al. (2008); Yao et al. (2019); Schlichtkrull et al. (2018)
 116 update each node by gathering information from its neighbors and then refining the node’s repre-
 117 sentation with that context. Stacking layers allows information to propagate over multiple hops, so
 118 nodes capture both local attributes and broader structural relations. When factor candidates are re-
 119 presented as graphs—such as trees for formulaic alphas—GNNs can encode semantic similarity and
 120 structural constraints more naturally than sequence models. This makes them attractive for learning
 121 embeddings of factors, guiding search over symbolic expressions, and measuring diversity at the
 122 representation level. Additional details appear in Appendix B.2.
 123

124 2.3 GENERATIVE FLOW NETWORKS

125 Generative Flow Networks (GFlowNets) Bengio et al. (2021); Malkin et al. (2022); Bengio et al.
 126 (2023) are generative learners that construct objects step by step and aim to sample a diverse set of
 127 high-reward solutions rather than collapsing to a single optimum. They treat generation as moving
 128 through a directed acyclic state space from an initial empty state to a terminal, valid object. By learn-
 129 ing complementary forward and backward policies and matching “flow” through states, GFlowNets
 130 approximate a sampling distribution that is shaped by the downstream reward. Practically, this yields
 131 exploration that is both reward-aware and diversity-seeking, producing a portfolio of candidates with
 132 varied structures and competitive quality—properties that are well aligned with the needs of alpha
 133 discovery and combination. Additional details appear in Appendix B.3.
 134

135 3 METHODOLOGY

136 3.1 FRAMEWORK OVERVIEW AND PROBLEM FORMULATION

137 The primary objective of automated alpha discovery is to navigate a vast, combinatorial search space
 138 \mathcal{X} of potential mathematical expressions, or ”alphas”. Each alpha $\alpha \in \mathcal{X}$ is a function that maps
 139 historical market data for a universe of N assets with M features at day d , denoted as $X_d \in \mathbb{R}^{N \times M}$,
 140 to a vector of predictive signals $z_d = \alpha(X_d) \in \mathbb{R}^N$. The quality of these signals is evaluated against
 141 future asset returns $y_d \in \mathbb{R}^N$.
 142

143 Existing RL frameworks model this as a sequential decision-making problem to construct a syner-
 144 gistic portfolio of alphas. In this paradigm, an agent iteratively generates new alphas to add to an
 145 evolving pool, \mathcal{F} . The reward for generating a new alpha, α_{new} , is its marginal contribution to the
 146 performance of a combination model $c(\cdot)$ trained on the updated pool. The objective at each step is
 147 to find a alpha that maximizes this improvement:
 148

$$\alpha_{\text{new}}^* = \arg \max_{\alpha \in \mathcal{X}} \mathbb{E} [R(\alpha | \mathcal{F})], \quad (1)$$

149 where the reward is defined as $R(\alpha | \mathcal{F}) = \text{IC}(c(X; \mathcal{F} \cup \{\alpha\})) - \text{IC}(c(X; \mathcal{F}))$. This formulation
 150 creates a non-stationary Markov Decision Process, as the reward for any given alpha changes when-
 151 ever the pool \mathcal{F}_t is updated. While this approach encourages synergy within the single, greedily
 152 constructed portfolio, it does not learn a global distribution over all high-quality alphas.
 153

154 We reformulate alpha discovery as a problem of learning a **generative policy** $P_\theta(\alpha)$ that directly
 155 models the distribution of high-quality alphas over the entire space \mathcal{X} . The policy is trained such
 156 that the probability of sampling any alpha is proportional to a carefully designed reward function
 157 $R(\alpha)$, which reflects its intrinsic quality and novelty:
 158

$$P_\theta(\alpha) \propto R(\alpha), \quad \forall \alpha \in \mathcal{X}, \quad (2)$$

159 By sampling from this learned global distribution, rather than following a single construction path,
 160 we can generate a more diverse and robust portfolio of candidate alphas.
 161

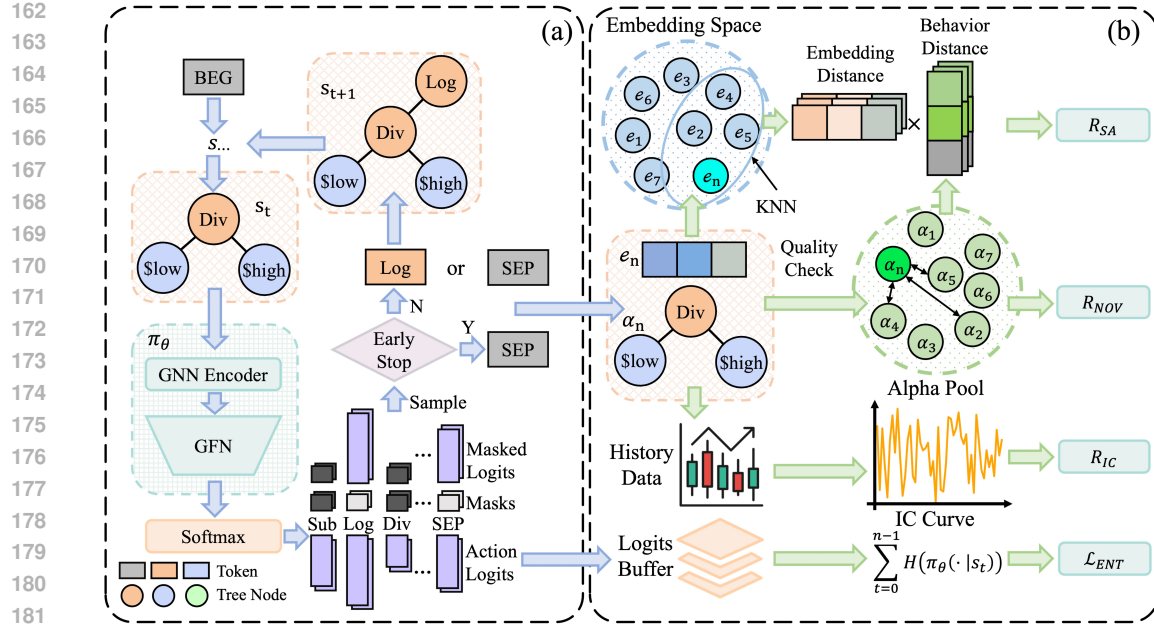


Figure 2: **An Overview of AlphaSAGE.** (a) **AlphaGenerator.** Starting from an empty state, a GNN encoder embeds the partial expression tree; a GFlowNet policy produces masked action logits over valid edits. We sample the next token, apply early stopping via a forced SEP when triggered, and continue until a terminal, valid alpha is formed. The resulting formula α_n and its embedding e_n are retained for evaluation. (b) **AlphaEvaluator.** Each α_n is scored with R_{SA} (embedding–behavior alignment), R_{NOV} (novelty vs. the existing alpha set), R_{IC} (predictive correlation), and an entropy regularizer \mathcal{L}_{ENT} (from the action-logit buffer). These components, together with the trajectory–balance term \mathcal{L}_{TB} , are aggregated into the final training objective.

3.2 ALPHA GENERATION VIA GENERATIVE FLOW NETWORKS

To address the need for a diverse portfolio, we propose a new framework with GFlowNets. A GFlowNet is a probabilistic generative model designed to learn a stochastic policy for sampling objects α from a space \mathcal{X} with probability $P(\alpha)$ proportional to a given reward function $R(\alpha)$.

The construction of an alpha is modeled as a trajectory $\tau = (s_0 \rightarrow s_1 \rightarrow \dots \rightarrow s_n = \alpha)$ in a state space represented as a directed acyclic graph (DAG).

- **States** ($s \in \mathcal{S}$): Partially constructed ASTs. The initial state s_0 is an empty tree. Terminal states are complete and valid ASTs, forming the space $\mathcal{X} \subset \mathcal{S}$.
- **Actions** ($a \in \mathcal{A}$): Adding a new token (operator or feature) to an open leaf node of a partial AST. According to the state s , invalid actions are masked and the next token is sampled from the masked distribution.
- **Complete Trajectories:** A full trajectory corresponds to constructing a valid expression tree. Only such trajectories are considered terminal and eligible for evaluation.

To prevent expressions from growing excessively long or from being forcefully terminated into invalid states after exceeding the maximum token length, we incorporate an **early stop** mechanism. Specifically, when the current stack already forms a valid expression, the generation process may stop with a probability:

$$p = \frac{\text{Len}(s_t)}{\text{MaxLen}}, \quad (3)$$

where $\text{Len}(s_t)$ is the number of nodes in s_t , and MaxLen is the maximum allowed length. This mechanism balances exploration of longer expressions with the efficiency of producing syntactically valid formulas.

216 A GFlowNet learns a forward policy $P_F(s_{t+1}|s_t; \theta)$ for constructing objects and a backward policy
 217 $P_B(s_t|s_{t+1}; \theta)$ for deconstruction. The training objective enforces a flow-matching condition
 218 throughout the state space, ensuring that the probability of generating a complete alpha α matches
 219 the target distribution:

$$220 \quad 221 \quad P(\alpha) = \sum_{\tau: s_n = \alpha} P_F(\tau) = \frac{R(\alpha)}{Z}, \quad (4)$$

222 where $Z = \sum_{\alpha' \in \mathcal{X}} R(\alpha')$ is a learnable parameter representing the total flow or partition function.
 223 While several loss functions exist, we use the Trajectory Balance (TB) loss, which is particularly
 224 suitable for our scenario as it focuses on full trajectories. The TB loss for a given trajectory τ is:
 225

$$226 \quad 227 \quad \mathcal{L}_{\text{TB}}(\tau) = \left(\log Z_\theta + \sum_{t=1}^n \log P_F(s_t|s_{t-1}; \theta) - \log R(s_n) - \sum_{t=1}^n \log P_B(s_{t-1}|s_t; \theta) \right)^2, \quad (5)$$

228 where Z_θ is a learnable scalar approximating total flow. Minimizing this loss over sampled trajectories
 229 trains the policy, resulting in a model that produces a diverse set of high-reward alphas.
 230

231 3.3 GNN EMBEDDING AND STRUCTURE-AWARE REWARD

232 A fundamental limitation of existing methods is their reliance on sequential encoders (e.g., LSTMs)
 233 operating on flattened representations like Reverse Polish Notation. Such an approach fails to cap-
 234 ture the hierarchical structure of mathematical expressions, treating logically equivalent formulas
 235 (e.g., *close* + *open* and *open* + *close*) as different sequences. To overcome this, we first parse every
 236 formulaic alpha α into its corresponding AST, denoted as $\mathcal{T}_\alpha = (\mathcal{V}_\alpha, \mathcal{E}_\alpha)$, where \mathcal{V}_α is the set of
 237 nodes (operators and features) and \mathcal{E}_α is the set of edges representing the computational hierarchy.
 238 This representation is invariant to semantically inconsequential syntactic variations.
 239

240 To capture the heterogeneity of relations between different types of operators and features in the
 241 \mathcal{T}_α , we adopt RGCN as the encoder. Unlike standard GNNs that treat all edges uniformly, RGCNs
 242 explicitly model multiple relation types, which is crucial for distinguishing, for example, the edge
 243 between a temporal operator and a feature versus the edge between a temporal operator and its
 244 window length.

245 Each node $v \in \mathcal{V}_\alpha$ is initialized with a feature vector $h_v^{(0)}$. At layer l , the hidden representation of
 246 node v is updated as:

$$247 \quad 248 \quad h_v^{(l)} = \text{ReLU} \left(\sum_{r \in \mathcal{R}} \sum_{u \in \mathcal{N}_r(v)} \frac{1}{c_{v,r}} W_r^{(l)} h_u^{(l-1)} + W_0^{(l)} h_v^{(l-1)} \right), \quad (6)$$

$$249 \quad e_\alpha = \text{MaxPooling}(\{h_v^{(L)}\}_{v \in \mathcal{V}_\alpha}), \quad (7)$$

250 where \mathcal{R} is the set of relation types, $\mathcal{N}_r(v)$ denotes the neighbors of node v connected via relation
 251 r , $c_{v,r}$ is a normalization constant (e.g., $|\mathcal{N}_r(v)|$), $W_r^{(l)}$ is the trainable weight matrix specific to
 252 relation r , and $W_0^{(l)}$ is a self-loop transformation matrix. This embedding provides a relation-aware
 253 and structure-aware representation of the alpha.

254 To ensure that the learned embedding is not just structurally aware but also predictive of the alpha's
 255 actual behavior, we introduce a Structure-Aware (SA) reward. The goal is to further ensure that
 256 alphas with similar structural embeddings exhibit similar behavioral patterns.
 257

258 Let $Z_i \in \mathbb{R}^{D \times N}$ be the time-series vector of cross-sectionally normalized outputs for α_i and $Z_i(d) \in$
 259 \mathbb{R}^N is the output at day d . We define a behavioral distance based on the outputs of α_i and α_j :

$$260 \quad 261 \quad d_{\text{behav}}(\alpha_i, \alpha_j) = \frac{1}{D} \sum_{d=1}^D (Z_i(d) - Z_j(d))^2, \quad (8)$$

$$262 \quad 263 \quad w_{ij} = \frac{\exp(-\|e_{\alpha_i} - e_{\alpha_j}\|^2)}{\sum_{k \in \mathcal{N}_K(\alpha_i)} \exp(-\|e_{\alpha_i} - e_{\alpha_k}\|^2)}, \quad j \in \mathcal{N}_K(\alpha_i), \quad (9)$$

$$264 \quad 265 \quad R_{\text{SA}}(\alpha_i) = \exp \left(- \sum_{j \in \mathcal{N}_K(\alpha_i)} w_{ij} \cdot d_{\text{behav}}(\alpha_i, \alpha_j) \right), \quad (10)$$

270 where $\mathcal{N}_K(\alpha_i)$ is K -nearest neighbors of α_i .
 271

272 **3.4 MULTI-FACETED REWARD FUNCTION AND TRAINING OBJECTIVE**
 273

274 The effectiveness of the GFlowNet is critically dependent on the design of the reward function
 275 $R(\alpha)$. To address reward sparsity and guide exploration effectively, we design a dense, multi-faceted
 276 reward function that dynamically combines several components.
 277

278 The total reward for a completed α at training step T is a weighted sum of three components:
 279

280 1. **Terminal Performance Reward** (R_{IC}): The primary measure of an alpha’s predictive
 281 power, defined as its Information Coefficient:

282
$$R_{\text{IC}}(\alpha) = \text{IC}(\alpha, y) = \left| \mathbb{E}_d \left[\frac{\text{Cov}(\alpha(X_d), y_d)}{\sqrt{\text{Var}(\alpha(X_d)) \cdot \text{Var}(y_d)}} \right] \right|. \quad (11)$$

 283

284 2. **Structure-Aware Reward** (R_{SA}): As defined in Eq. 10, this reward provides a dense signal
 285 for aligning the alpha’s structural embedding with its behavior.
 286 3. **Novelty Reward** (R_{NOV}): To encourage the discovery of novel alphas, we introduce a nov-
 287 elty reward. It penalizes similarity to a dynamically updated library $\mathcal{F}_{\text{known}}$ of previously
 288 discovered high-quality alphas. The definition is:
 289

290
$$R_{\text{NOV}}(\alpha) = 1 - \max_{\alpha' \in \mathcal{F}_{\text{known}}} |\text{IC}(\alpha, \alpha')|. \quad (12)$$

 291

292 These reward components are combined using a time-dependent weighting scheme to balance dif-
 293 ferent objectives throughout the training process. The final reward function is:
 294

295
$$R(\alpha, T) = R_{\text{IC}}(\alpha) + \lambda(T)R_{\text{SA}}(\alpha) + \eta(T)R_{\text{NOV}}(\alpha), \quad (13)$$

 296

297 where $\lambda(T) = (1 - \frac{T}{T_{\text{anneal}}}) \cdot \lambda_{\text{max}}$ is a scheduling function that gradually decreases the weight of the
 298 structure-aware reward, and $\eta(T) = (1 - \frac{t}{T_{\text{anneal}}}) \cdot \eta_{\text{max}}$ is a weight for the novelty reward.
 299

300 Furthermore, to prevent premature convergence and encourage fine-grained exploration at the action
 301 level, we add a policy entropy bonus to our final training objective. The objective is to minimize the
 302 expected Trajectory Balance loss regularized by the entropy of the forward policy:
 303

304
$$\mathcal{L}_{\text{ENT}} = -\mathbb{E}_{\tau \sim P_F(\tau; \theta)} \left[\sum_{t=0}^{n-1} H(\pi_\theta(\cdot | s_t)) \right], \quad (14)$$

 305

306
$$\mathcal{L}_{\text{final}} = \mathbb{E}_{\tau \sim P_F(\tau; \theta)} [\mathcal{L}_{\text{TB}}(\tau)] + \beta \cdot \mathcal{L}_{\text{ENT}}, \quad (15)$$

 307

308 where $H(\pi_\theta(\cdot | s_t))$ is the entropy of the action selection policy at state s_t and β is a hyperparameter
 309 controlling the strength of the entropy regularization. This comprehensive objective guides Al-
 310 phaSAGE to learn a generative policy that produces a diverse, novel, and highly predictive portfolio
 311 of alpha alphas.
 312

313 **3.5 ALPHA COMBINATION**
 314

315 For the combination stage, we follow the approach proposed in *AlphaForge* Shi et al. (2025a).
 316 Specifically, instead of fixing a static set of alphas, the framework performs a dynamic re-selection
 317 and linear combination of mined alphas. At each period, recently effective alphas are filtered and
 318 re-weighted through simple linear regression, yielding a time-varying “Mega-Alpha.”
 319

320 This design is advantageous because it adapts quickly to regime shifts while maintaining inter-
 321 pretability: alpha contributions remain transparent, and the portfolio avoids overfitting by discard-
 322 ing stale or redundant signals. Compared with complex non-linear combiners, this method offers a
 323 balance between robustness, efficiency, and explanatory clarity.

324 4 EXPERIMENTS AND RESULTS

325 4.1 EXPERIMENT SETTING

326 **Evaluation Metrics.** Based on prior work [Yu et al. \(2023\)](#); [Tang et al. \(2025\)](#) and real-world
 327 trading scenarios, we employed two types of metrics for model evaluation.(1): **Correlation Metrics**,
 328 including Information Coefficient (IC), IC Information Ratio (ICIR), Rank Information Coefficient
 329 (RIC), RIC Information Ratio (RICIR); (2): **Portfolio Metrics**, including Annualized Return (AR),
 330 Maximum Drawdown (MDD), Sharpe Ratio (SR). All metrics are better when higher. Detailed
 331 definitions and backtest settings are provided in the Appendix [C.1](#).
 332

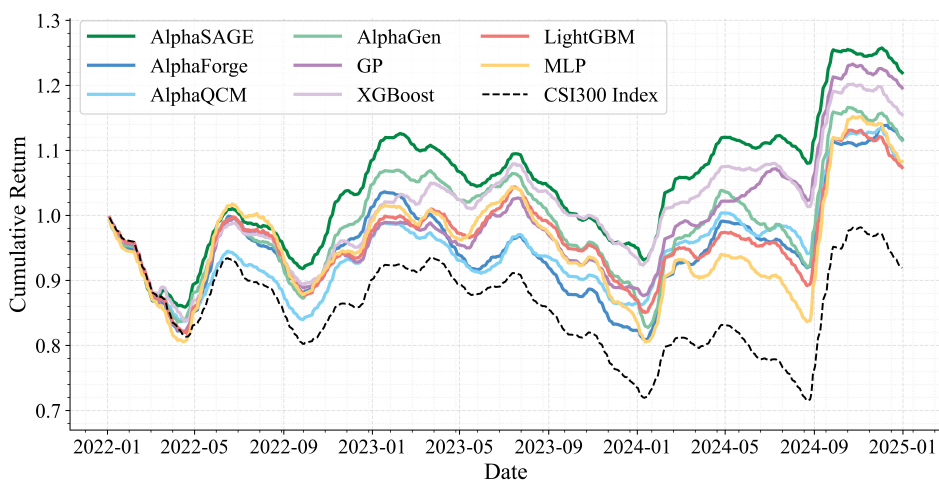
333 **Datasets.** We selected three important subsets from two major markets [Yang et al. \(2020\)](#): the
 334 CSI300 and CSI500 in the Chinese market, and the S&P500 in the U.S. market. The split of the
 335 training set/validation set/test set for the Chinese market is defined as follows: 2010-01-01 to 2020-
 336 12-31 / 2021-01-01 to 2021-12-31 / 2022-01-01 to 2024-12-31. For the US market: 2010-01-01
 337 to 2016-12-31 / 2017-01-01 to 2017-12-31 / 2018-01-01 to 2020-12-31.² Detailed hyperparameter
 338 settings are provided in Appendix [C.2](#).
 339

340 **Baselines.** We compare AlphaSAGE with several baseline approaches: (1) Traditional machine
 341 learning methods include **MLP** [Murtagh \(1991\)](#), **LightGBM** [Ke et al. \(2017\)](#), and **XGBoost** [Chen
 342 & Guestrin \(2016\)](#); (2) GA-based methods include **GP** [Chen et al. \(2021\)](#); (3) RL-based methods
 343 include **AlphaGen** [Yu et al. \(2023\)](#) and **AlphaQCM** [Zhu & Zhu \(2025\)](#); (4) Generative adversarial
 344 networks-based methods include **AlphaForge** [Shi et al. \(2025a\)](#). The details of baseline are available
 345 at Appendix [C.3](#).
 346

347 4.2 OVERALL PERFORMANCE

348 Table 1 summarizes results across CSI300/500 and S&P500: AlphaSAGE ranks first on all cor-
 349 relation metrics, with notably higher ICIR/RICIR, and these gains translate into the best portfolio
 350 outcomes (highest annualized return, lowest drawdown, highest Sharpe).
 351

352 Figure 3 further shows that on CSI300 (2022–2024) AlphaSAGE maintains a persistent lead in
 353 cumulative returns, with smoother drawdowns, faster recoveries, and stronger rebound capture; the
 354 CSI300 index lags throughout, underscoring the value of active factor discovery and combination.
 355



356 Figure 3: Cumulative return on CSI300 (2022–2024). Comparison among AlphaSAGE (ours), all
 357 baselines, and CSI300 Index benchmark.
 358

359 ²Due to limitations in the data source, the US market data used in this study concludes on 2020-12-31.
 360

378
 379 Table 1: Performance Comparison of Different Methods on CSI 300, CSI 500 (China) and S&P500
 380 (U.S.). Bold and underlined numbers represent the best and second-best performance across all
 381 compared approaches, respectively.

382 Dataset	383 Method	384 Correlation Metrics				385 Portfolio Metrics		
		386 <i>IC</i>	387 <i>ICIR</i>	388 <i>RIC</i>	389 <i>RICIR</i>	390 <i>AR</i>	391 <i>MDD</i>	392 <i>SR</i>
393 CSI300	394 MLP	0.020	0.158	0.019	0.142	3.54%	-20.9%	0.68
	395 LightGBM	0.011	0.124	0.006	0.064	2.61%	-18.5%	0.53
	396 XGBoost	0.031	0.243	0.033	0.248	5.40%	<u>-17.5%</u>	1.26
	397 GP	0.026	0.215	0.028	0.216	<u>6.80%</u>	-17.6%	<u>1.55</u>
	398 AlphaGen	<u>0.058</u>	<u>0.414</u>	<u>0.057</u>	<u>0.360</u>	4.00%	-22.6%	0.76
	399 AlphaQCM	0.043	0.262	0.042	0.246	1.95%	-24.8%	0.36
	400 AlphaForge	0.041	0.259	0.052	0.306	3.90%	-21.9%	0.88
	401 AlphaSAGE(ours)	0.079	0.496	0.094	0.583	7.62%	-17.3%	1.71
402 CSI500	403 MLP	0.017	0.185	0.020	0.233	1.56%	-24.3%	0.27
	404 LightGBM	0.024	0.305	0.021	0.264	4.61%	-17.5%	0.89
	405 XGBoost	0.039	0.365	0.052	0.528	<u>5.50%</u>	-17.1%	1.15
	406 GP	0.014	0.238	0.022	0.233	3.04%	-19.4%	0.56
	407 AlphaGen	0.032	0.270	0.031	0.230	<u>1.15%</u>	-32.4%	0.19
	408 AlphaQCM	0.048	<u>0.378</u>	0.073	0.546	4.06%	-24.0%	0.75
	409 AlphaForge	<u>0.053</u>	0.345	<u>0.083</u>	0.600	4.18%	<u>-16.7%</u>	0.93
	410 AlphaSAGE(ours)	0.054	0.379	0.084	0.637	5.53%	-16.0%	1.20
411 S&P500	412 MLP	0.035	0.287	0.020	0.143	12.85%	-5.6%	3.35
	413 LightGBM	0.023	0.196	0.018	0.165	11.11%	-5.1%	4.22
	414 XGBoost	0.016	0.159	0.026	0.168	13.25%	-8.3%	3.61
	415 GP	0.032	0.308	0.002	0.016	13.39%	-13.0%	3.15
	416 AlphaGen	<u>0.044</u>	0.396	0.013	0.127	10.31%	-5.5%	3.96
	417 AlphaQCM	0.038	0.262	0.010	0.071	13.86%	-13.0%	3.30
	418 AlphaForge	0.039	<u>0.422</u>	<u>0.031</u>	0.324	<u>17.24%</u>	<u>-5.0%</u>	<u>6.30</u>
	419 AlphaSAGE(ours)	0.052	0.493	0.038	0.382	19.47%	-4.2%	6.32

4.3 ABLATION STUDY

420
 421 Table 2 shows that the plain GFlowNet baseline is weakest; adding only early stopping (ES) further
 422 hurts, implying ES needs a stronger encoder. Replacing the sequence encoder with a GNN provides
 423 the largest single lift across correlation and risk metrics, underscoring the value of structure-aware
 424 representations. Adding the structure-aware reward (SA) improves ranking stability (ICIR/RICIR)
 425 and tightens drawdowns. Introducing the novelty reward (NOV) raises both signal quality and trad-
 426 ability by reducing redundancy among factors. Finally, the entropy regularizer (ENT) yields the
 427 best overall results—higher IC/RIC, AR, and Sharpe with controlled MDD—indicating improved
 428 exploration without brittleness and supporting the method’s robustness to component choices.

429
 430 Table 2: Ablation study on CSI300. The base model is GflowNets, where ES denotes Early Stop-
 431 ping, GNN indicates whether a GNN or LSTM is used as the encoder, SA stands for Structure-Aware
 432 Reward, NOV represents Novelty Reward, and ENT denotes Entropy Loss.

433	434 Included Components					435 Correlation Metrics				436 Portfolio Metrics		
	437 ES	438 GNN	439 SA	440 NOV	441 ENT	442 <i>IC</i>	443 <i>ICIR</i>	444 <i>RIC</i>	445 <i>RICIR</i>	446 <i>AR</i>	447 <i>MDD</i>	448 <i>SR</i>
449 <input checked="" type="checkbox"/>	450 <input checked="" type="checkbox"/>	451 <input checked="" type="checkbox"/>	452 <input checked="" type="checkbox"/>	453 <input checked="" type="checkbox"/>	454 <input checked="" type="checkbox"/>	455 0.048	456 0.393	457 0.057	458 0.437	459 3.63%	460 -22.9%	461 0.72
462 <input checked="" type="checkbox"/>	463 <input checked="" type="checkbox"/>	464 <input checked="" type="checkbox"/>	465 <input checked="" type="checkbox"/>	466 <input checked="" type="checkbox"/>	467 <input checked="" type="checkbox"/>	468 0.046	469 0.313	470 0.060	471 0.397	472 -0.47%	473 -24.8%	474 -0.11
475 <input checked="" type="checkbox"/>	476 <input checked="" type="checkbox"/>	477 <input checked="" type="checkbox"/>	478 <input checked="" type="checkbox"/>	479 <input checked="" type="checkbox"/>	480 <input checked="" type="checkbox"/>	481 0.070	<u>0.495</u>	483 0.088	484 0.554	485 5.58%	486 -19.4%	487 1.25
488 <input checked="" type="checkbox"/>	489 <input checked="" type="checkbox"/>	490 <input checked="" type="checkbox"/>	491 <input checked="" type="checkbox"/>	492 <input checked="" type="checkbox"/>	493 <input checked="" type="checkbox"/>	494 0.071	495 0.453	496 0.088	497 0.566	498 4.68%	<u>-17.6%</u>	499 1.14
500 <input checked="" type="checkbox"/>	501 <input checked="" type="checkbox"/>	502 <input checked="" type="checkbox"/>	503 <input checked="" type="checkbox"/>	504 <input checked="" type="checkbox"/>	505 <input checked="" type="checkbox"/>	506 0.075	507 0.494	<u>0.092</u>	0.614	<u>6.77%</u>	-17.8%	<u>1.53</u>
507 <input checked="" type="checkbox"/>	508 <input checked="" type="checkbox"/>	509 <input checked="" type="checkbox"/>	510 <input checked="" type="checkbox"/>	511 <input checked="" type="checkbox"/>	512 <input checked="" type="checkbox"/>	0.079	0.496	0.094	0.583	7.62%	-17.3%	1.71

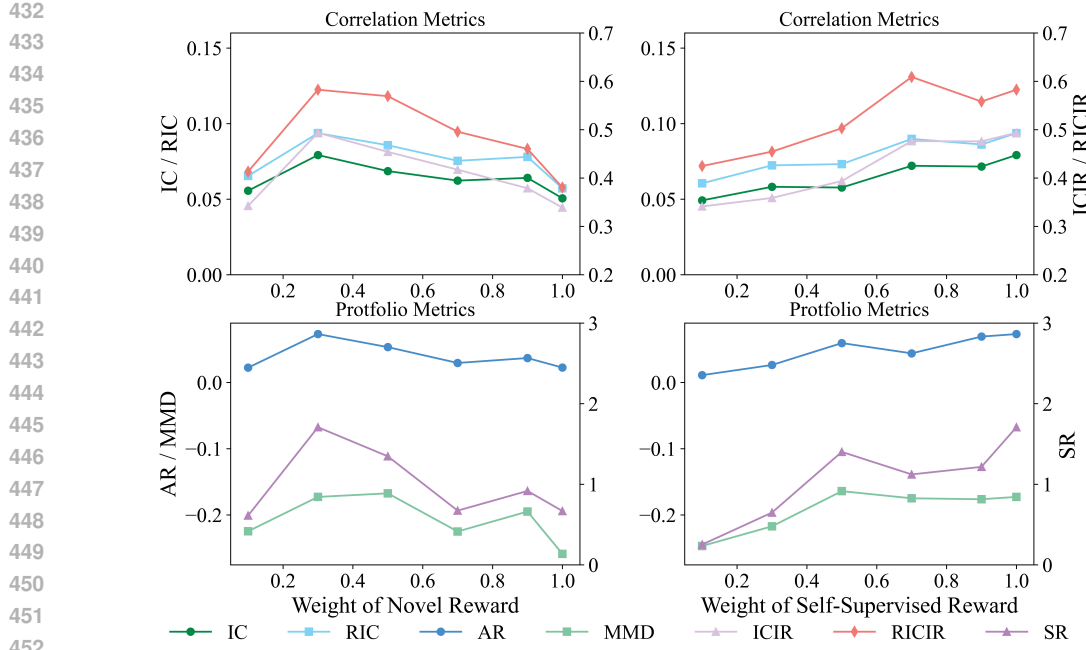


Figure 4: Sensitivity analysis of the weights for R_{NOV} and R_{SA} on CSI300. For the y-axis, IC, RIC, AR, and MDD refer to the axis on the left; ICIR, RICIR, and SR refer to the axis on the right.

4.4 SENSITIVITY ANALYSIS

We vary the weights of novelty reward (R_{NOV}) and structure-aware reward (R_{SA}) on CSI300 (Fig. 4). For R_{NOV} , correlation and portfolio metrics improve at small–moderate levels and remain on a broad plateau before tapering when novelty dominates. For R_{SA} , improvements are largely monotonic across correlation and portfolio metrics with stable drawdowns. Overall, AlphaSAGE exhibits smooth responses without abrupt performance drops, indicating robustness to a wide range of hyperparameter choices and low sensitivity around the operating region.

5 CONCLUSION

We introduced AlphaSAGE, a structure-aware, diversity-seeking framework for formulaic alpha discovery and combination. The approach unifies a GNN encoder for symbolic expressions, a GFlowNet generator that explores multiple high-reward modes, and a multi-signal training objective coupling predictive quality, representation–behavior alignment, novelty pressure, and entropy-based regularization. A transparent, dynamic linear combiner then translates candidate alphas into a tradable portfolio signal while maintaining interpretability.

Empirically, AlphaSAGE delivers first-rank correlation metrics across CSI300/500 and S&P500 and consistently converts these gains into superior portfolio outcomes. On CSI300 (2022–2024), its cumulative return curve maintains a persistent lead with smoother drawdowns, faster recoveries, and stronger rebound capture, underscoring robust generalization across market regimes. Ablations attribute the largest single lift to structure-aware encoding (GNN), with self-supervised alignment improving rank stability and risk control, novelty rewarding useful diversity that lifts both signal quality and tradability, and entropy regularization sharpening exploration without brittleness. Sensitivity studies show smooth responses over broad ranges of the novelty and alignment weights, indicating low tuning burden and practical robustness.

Together, these results demonstrate that coupling structure-aware representation, diversity-seeking generation, and principled multi-signal supervision yields reliable improvements in both signal quality and its conversion to realized returns, while preserving transparency in how factors are generated and combined.

486 REFERENCES
487

488 Emmanuel Bengio, Moksh Jain, Maksym Korablyov, Doina Precup, and Yoshua Bengio. Flow
489 network based generative models for non-iterative diverse candidate generation. *Advances in
490 neural information processing systems*, 34:27381–27394, 2021.

491 Yoshua Bengio, Salem Lahlou, Tristan Deleu, Edward J Hu, Mo Tiwari, and Emmanuel Bengio.
492 Gflownet foundations. *Journal of Machine Learning Research*, 24(210):1–55, 2023.
493

494 Michael M Bronstein, Joan Bruna, Taco Cohen, and Petar Veličković. Geometric deep learning:
495 Grids, groups, graphs, geodesics, and gauges. *arXiv preprint arXiv:2104.13478*, 2021.
496

497 Lang Cao, Zekun Xi, Long Liao, Ziwei Yang, and Zheng Cao. Chain-of-alpha: Unleashing
498 the power of large language models for alpha mining in quantitative trading. *arXiv preprint
499 arXiv:2508.06312*, 2025.

500 Dangxing Chen. Can i trust the explanations? investigating explainable machine learning methods
501 for monotonic models. *arXiv preprint arXiv:2309.13246*, 2023.
502

503 Tianqi Chen and Carlos Guestrin. XGBoost: A scalable tree boosting system. In *Proceedings of
504 the 22nd ACM SIGKDD International Conference on Knowledge Discovery and Data Mining*,
505 pp. 785–794. ACM, 2016. ISBN 978-1-4503-4232-2. doi: 10.1145/2939672.2939785. URL
506 <https://dl.acm.org/doi/10.1145/2939672.2939785>.

507 Tianxiang Chen, Wei Chen, and Luyao Du. An empirical study of financial factor mining based
508 on gene expression programming. In *2021 4th International Conference on Advanced Electronic
509 Materials, Computers and Software Engineering (AEMCSE)*, pp. 1113–1117. IEEE, 2021.
510

511 Wei-Lin Chiang, Xuanqing Liu, Si Si, Yang Li, Samy Bengio, and Cho-Jui Hsieh. Cluster-gcn:
512 An efficient algorithm for training deep and large graph convolutional networks. In *Proceedings
513 of the 25th ACM SIGKDD international conference on knowledge discovery & data mining*, pp.
514 257–266, 2019.

515 Can Cui, Wei Wang, Meihui Zhang, Gang Chen, Zhaojing Luo, and Beng Chin Ooi. AlphaEvolve:
516 A learning framework to discover novel alphas in quantitative investment. In *Proceedings of the
517 2021 International Conference on Management of Data*, pp. 2208–2216. ACM, 2021. ISBN 978-
518 1-4503-8343-1. doi: 10.1145/3448016.3457324. URL [https://dl.acm.org/doi/10.1145/3448016.
519 3457324](https://dl.acm.org/doi/10.1145/3448016.3457324).
520

521 Justin Gilmer, Samuel S Schoenholz, Patrick F Riley, Oriol Vinyals, and George E Dahl. Neural
522 message passing for quantum chemistry. In *International conference on machine learning*, pp.
523 1263–1272. Pmlr, 2017.

524 Will Hamilton, Zhitao Ying, and Jure Leskovec. Inductive representation learning on large graphs.
525 *Advances in neural information processing systems*, 30, 2017.
526

527 Weihua Hu, Matthias Fey, Marinka Zitnik, Yuxiao Dong, Hongyu Ren, Bowen Liu, Michele Catasta,
528 and Jure Leskovec. Open graph benchmark: Datasets for machine learning on graphs. *Advances
529 in neural information processing systems*, 33:22118–22133, 2020.

530 Moksh Jain, Emmanuel Bengio, Alex Hernandez-Garcia, Jarrid Rector-Brooks, Bonaventure FP
531 Dossou, Chanakya Ajit Ekbote, Jie Fu, Tianyu Zhang, Michael Kilgour, Dinghuai Zhang, et al.
532 Biological sequence design with gflownets. In *International Conference on Machine Learning*,
533 pp. 9786–9801. PMLR, 2022.
534

535 Zura Kakushadze. 101 formulaic alphas, 2016. URL <https://arxiv.org/abs/1601.00991>.
536

537 Guolin Ke, Qi Meng, Thomas Finley, Taifeng Wang, Wei Chen, Weidong Ma, Qiwei Ye, and Tie-Yan
538 Liu. LightGBM: A highly efficient gradient boosting decision tree. In *Advances in Neural Infor-
539 mation Processing Systems*, volume 30. Curran Associates, Inc., 2017. URL [https://proceedings.
neurips.cc/paper_files/paper/2017/hash/6449f44a102fde848669bdd9eb6b76fa-Abstract.html](https://proceedings.neurips.cc/paper_files/paper/2017/hash/6449f44a102fde848669bdd9eb6b76fa-Abstract.html).

540 Salem Lahiou, Tristan Deleu, Pablo Lemos, Dinghuai Zhang, Alexandra Volokhova, Alex
 541 Hernández-García, Léna Néhale Ezzine, Yoshua Bengio, and Nikolay Malkin. A theory of
 542 continuous generative flow networks. In *International Conference on Machine Learning*, pp. 18269–
 543 18300. PMLR, 2023.

544 Yann LeCun, Sumit Chopra, Raia Hadsell, M Ranzato, Fujie Huang, et al. A tutorial on energy-
 545 based learning. *Predicting structured data*, 1(0), 2006.

546 Pan Li, Yanbang Wang, Hongwei Wang, and Jure Leskovec. Distance encoding: Design provably
 547 more powerful neural networks for graph representation learning. *Advances in Neural Information
 548 Processing Systems*, 33:4465–4478, 2020.

549 Zhiwei Li, Ran Song, Caihong Sun, Wei Xu, Zhengtao Yu, and Ji-Rong Wen. Can large language
 550 models mine interpretable financial factors more effectively? a neural-symbolic factor mining
 551 agent model. In Lun-Wei Ku, Andre Martins, and Vivek Srikumar (eds.), *Findings of the Asso-
 552 ciation for Computational Linguistics: ACL 2024*, pp. 3891–3902, Bangkok, Thailand, August
 553 2024. Association for Computational Linguistics. doi: 10.18653/v1/2024.findings-acl.233. URL
 554 <https://aclanthology.org/2024.findings-acl.233/>.

555 Kanika Madan, Jarrid Rector-Brooks, Maksym Korablyov, Emmanuel Bengio, Moksh Jain, An-
 556 drei Cristian Nica, Tom Bosc, Yoshua Bengio, and Nikolay Malkin. Learning gflownets from
 557 partial episodes for improved convergence and stability. In *International Conference on Machine
 558 Learning*, pp. 23467–23483. PMLR, 2023.

559 Nikolay Malkin, Moksh Jain, Emmanuel Bengio, Chen Sun, and Yoshua Bengio. Trajectory balance:
 560 Improved credit assignment in gflownets. *Advances in Neural Information Processing Systems*,
 561 35:5955–5967, 2022.

562 Fionn Murtagh. Multilayer perceptrons for classification and regression. *Neurocomputing*, 2(5-6):
 563 183–197, 1991.

564 Junji Ren, Junjie Zhao, Shengcai Liu, and Peng Yang. From Linear to Hierarchical: Evolving Tree-
 565 structured Thoughts for Efficient Alpha Mining, August 2025. URL <http://arxiv.org/abs/2508.16334> [cs].

566 arXiv:2508.16334 [cs].

567 Tim Salimans, Diederik Kingma, and Max Welling. Markov chain monte carlo and variational
 568 inference: Bridging the gap. In *International conference on machine learning*, pp. 1218–1226.
 569 PMLR, 2015.

570 Franco Scarselli, Marco Gori, Ah Chung Tsoi, Markus Hagenbuchner, and Gabriele Monfardini.
 571 The graph neural network model. *IEEE transactions on neural networks*, 20(1):61–80, 2008.

572 Michael Schlichtkrull, Thomas N Kipf, Peter Bloem, Rianne Van Den Berg, Ivan Titov, and Max
 573 Welling. Modeling relational data with graph convolutional networks. In *European semantic web
 574 conference*, pp. 593–607. Springer, 2018.

575 Hao Shi, Weili Song, Xinting Zhang, Jiahe Shi, Cuicui Luo, Xiang Ao, Hamid Arian, and Luis Angel
 576 Seco. Alphaforge: A framework to mine and dynamically combine formulaic alpha factors. In
 577 Toby Walsh, Julie Shah, and Zico Kolter (eds.), *AAAI-25, Sponsored by the Association for the
 578 Advancement of Artificial Intelligence, February 25 - March 4, 2025, Philadelphia, PA, USA*, pp.
 579 12524–12532. AAAI Press, 2025a. doi: 10.1609/AAAI.V39I12.33365. URL <https://doi.org/10.1609/aaai.v39i12.33365>.

580 Yu Shi, Yitong Duan, and Jian Li. Navigating the alpha jungle: An llm-powered mcts framework
 581 for formulaic factor mining. *arXiv preprint arXiv:2505.11122*, 2025b.

582 Ziyi Tang, Zechuan Chen, Jiarui Yang, Jiayao Mai, Yongsen Zheng, Keze Wang, Jinrui Chen, and
 583 Liang Lin. Alphaagent: Llm-driven alpha mining with regularized exploration to counteract alpha
 584 decay. In *Proceedings of the 31st ACM SIGKDD Conference on Knowledge Discovery and Data
 585 Mining V*, 2, pp. 2813–2822, 2025.

586 Petar Veličković, Guillem Cucurull, Arantxa Casanova, Adriana Romero, Pietro Lio, and Yoshua
 587 Bengio. Graph attention networks. *arXiv preprint arXiv:1710.10903*, 2017.

594 Feng Xu, Yan Yin, Xinyu Zhang, Tianyuan Liu, Shengyi Jiang, and Zongzhang Zhang.
 595 $\$\\text{Alpha}^2$$: Discovering Logical Formulaic Alphas using Deep Reinforcement Learning,
 596 June 2024. URL <http://arxiv.org/abs/2406.16505>. arXiv:2406.16505 [cs, q-fin].
 597

598 Keyulu Xu, Weihua Hu, Jure Leskovec, and Stefanie Jegelka. How powerful are graph neural
 599 networks? In *International Conference on Learning Representations*.
 600

601 Xiao Yang, Weiqing Liu, Dong Zhou, Jiang Bian, and Tie-Yan Liu. Qlib: An ai-oriented quantitative
 602 investment platform, 2020. URL <https://arxiv.org/abs/2009.11189>.
 603

604 Liang Yao, Chengsheng Mao, and Yuan Luo. Graph convolutional networks for text classification.
 605 In *Proceedings of the AAAI conference on artificial intelligence*, volume 33, pp. 7370–7377, 2019.
 606

607 Shuo Yu, Hongyan Xue, Xiang Ao, Feiyang Pan, Jia He, Dandan Tu, and Qing He. Generating
 608 synergistic formulaic alpha collections via reinforcement learning. In *Proceedings of the 29th
 609 ACM SIGKDD Conference on Knowledge Discovery and Data Mining*, 2023. doi: 10.1145/
 610 3580305.3599831.
 611

612 Dinghuai Zhang, Hanjun Dai, Nikolay Malkin, Aaron C Courville, Yoshua Bengio, and Ling Pan.
 613 Let the flows tell: Solving graph combinatorial problems with gflownets. *Advances in neural
 614 information processing systems*, 36:11952–11969, 2023.
 615

616 Tianping Zhang, Yuanqi Li, Yifei Jin, and Jian Li. AutoAlpha: an efficient hierarchical evolutionary
 617 algorithm for mining alpha factors in quantitative investment, 2020. URL <http://arxiv.org/abs/2002.08245>.
 618

619 Junjie Zhao, Chengxi Zhang, Min Qin, and Peng Yang. QuantFactor REINFORCE: Mining Steady
 620 Formulaic Alpha Factors with Variance-bounded REINFORCE, October 2024. URL <http://arxiv.org/abs/2409.05144>. arXiv:2409.05144.
 621

622 Junjie Zhao, Chengxi Zhang, Chenkai Wang, and Peng Yang. Learning from expert factors:
 623 Trajectory-level reward shaping for formulaic alpha mining, 2025. URL <https://arxiv.org/abs/2507.20263>.
 624

625 Da Zheng, Chao Ma, Minjie Wang, Jinjing Zhou, Qidong Su, Xiang Song, Quan Gan, Zheng Zhang,
 626 and George Karypis. Distdgl: Distributed graph neural network training for billion-scale graphs.
 627 In *2020 IEEE/ACM 10th Workshop on Irregular Applications: Architectures and Algorithms
 628 (IA3)*, pp. 36–44. IEEE, 2020.
 629

630 Zhoufan Zhu and Ke Zhu. Alphaqcm: Alpha discovery in finance with distributional reinforcement
 631 learning. In *Forty-second International Conference on Machine Learning*, 2025.
 632

633

634

635

636

637

638

639

640

641

642

643

644

645

646

647

648 A THE USE OF LARGE LANGUAGE MODELS (LLMs)
649650 We declare that the use of large language models (LLMs) during the drafting of this manuscript was
651 confined to language-related assistance, such as sentence refinement and grammatical corrections.
652 All substantive content was independently authored by the authors and underwent rigorous review
653 and verification following any modifications based on LLM assistance. This research did not involve
654 any other processes reliant upon large language models.
655656 B SUPPLEMENTARY BACKGROUND ON RELATED WORK
657658 B.1 ALPHA MINING AND COMBINATION
659660 **Search paradigms.** Early work emphasized manual, hypothesis-driven construction of formulaic
661 alphas; automated search later expanded with genetic algorithms (mutation/crossover over expres-
662 sion trees) [Chen et al. \(2021\)](#); [Zhang et al. \(2020\)](#); [Cui et al. \(2021\)](#) and reinforcement learning
663 (sequential decision-making over token spaces) [Yu et al. \(2023\)](#); [Zhu & Zhu \(2025\)](#); [Zhao et al.](#)
664 ([2024](#)); [Xu et al. \(2024\)](#). In addition, there are also approaches based on Large Language Models
665 (LLMs) [Cao et al. \(2025\)](#); [Shi et al. \(2025b\)](#); [Tang et al. \(2025\)](#); [Li et al. \(2024\)](#); [Chen \(2023\)](#); [Ren](#)
666 [et al. \(2025\)](#) that generate alphas using LLMs or refine existing alphas .
667668 **Combination and multicollinearity.** Given a library $\{z_{i,t}^{(k)}\}_{k=1}^K$, linear combination remains
669 prevalent for transparency:

670
$$s_{i,t} = \sum_{k=1}^K w_k z_{i,t}^{(k)}, \quad \mathbf{w} \in \mathbb{R}^K. \quad (16)$$

671

672 However, high cross-alpha correlation inflates estimator variance. Regularization and constraints
673 mitigate this:

674
$$\min_{\mathbf{w}} \sum_t \left\| \mathbf{y}_{t+\Delta} - Z_t \mathbf{w} \right\|_2^2 + \lambda_2 \|\mathbf{w}\|_2^2 + \lambda_1 \|\mathbf{w}\|_1 \quad \text{s.t. } \mathbf{1}^\top \mathbf{w} = 1, \quad \|\mathbf{w}\|_0 \leq s, \quad (17)$$

675

676 where $Z_t = [z_{\cdot,t}^{(1)}, \dots, z_{\cdot,t}^{(K)}]$ stacks alpha columns, and optional constraints control turnover or
677 exposure. Diagnostics such as condition number or VIF help monitor collinearity. Beyond static
678 weights, practice often uses rolling or regime-conditioned reweighting.
679680 B.2 GRAPH NEURAL NETWORKS (GNNs)
681682 **Message passing view.** A broad class of GNNs can be written as
683

684
$$\mathbf{m}_{u \rightarrow v}^{(\ell)} = \phi_{\text{msg}}^{(\ell)}(\mathbf{h}_u^{(\ell)}, \mathbf{h}_v^{(\ell)}, \mathbf{e}_{uv}), \quad \mathbf{a}_v^{(\ell)} = \square_{u \in \mathcal{N}(v)} \mathbf{m}_{u \rightarrow v}^{(\ell)}, \quad \mathbf{h}_v^{(\ell+1)} = \phi_{\text{upd}}^{(\ell)}(\mathbf{h}_v^{(\ell)}, \mathbf{a}_v^{(\ell)}), \quad (18)$$

685

686 where \square is a permutation-invariant aggregator (sum/mean/max or attention). Classical instances
687 include GCN [Yao et al. \(2019\)](#), GraphSAGE [Hamilton et al. \(2017\)](#), GAT [Veličković et al. \(2017\)](#),
688 GIN [Xu et al.](#), the MPNN family [Gilmer et al. \(2017\)](#), and relational/heterogeneous variants (R-
689 GCN) [Schlichtkrull et al. \(2018\)](#).
690691 **Spectral perspective (GCN).** Let $\hat{A} = A + I$ and $\hat{D} = \text{diag}(\sum_j \hat{A}_{ij})$. The layerwise propagation
692 is
693

$$H^{(\ell+1)} = \sigma(\hat{D}^{-1/2} \hat{A} \hat{D}^{-1/2} H^{(\ell)} W^{(\ell)}), \quad (19)$$

694 interpretable as a low-pass filter on the graph. Repeated smoothing risks *over-smoothing*, where
695 node embeddings become indistinguishable; residual connections, normalization, and careful depth
696 mitigate this [Bronstein et al. \(2021\)](#).
697698 **Attention and heterogeneity.** GAT computes attention weights α_{uv} over neighbors:
699

700
$$\alpha_{uv} = \frac{\exp(\text{LeakyReLU}(\mathbf{a}^\top [\mathbf{W} \mathbf{h}_u \parallel \mathbf{W} \mathbf{h}_v]))}{\sum_{w \in \mathcal{N}(v)} \exp(\text{LeakyReLU}(\mathbf{a}^\top [\mathbf{W} \mathbf{h}_w \parallel \mathbf{W} \mathbf{h}_v]))}, \quad \mathbf{h}'_v = \sigma \left(\sum_{u \in \mathcal{N}(v)} \alpha_{uv} \mathbf{W} \mathbf{h}_u \right). \quad (20)$$

701

702 R-GCN introduces relation-specific parameters:
 703

$$704 \quad \mathbf{h}_v^{(\ell+1)} = \sigma \left(\sum_{r \in \mathcal{R}} \sum_{u \in \mathcal{N}_r(v)} \frac{1}{c_{v,r}} W_r^{(\ell)} \mathbf{h}_u^{(\ell)} + W_0^{(\ell)} \mathbf{h}_v^{(\ell)} \right). \quad (21)$$

705
 706

707 **Expressivity and readout.** GIN links message passing to Weisfeiler–Lehman tests and uses a
 708 sum-aggregation MLP to approach maximal discriminative power in the 1-WL regime [Xu et al.](#).
 709 Graph-level outputs use readouts
 710

$$711 \quad \mathbf{h}_G = \text{READOUT}(\{\mathbf{h}_v^{(L)}\}_{v \in G}), \quad \text{e.g., sum/mean/max.} \quad (22)$$

712

713 Positional or structural encodings (e.g., Laplacian eigenvectors, distance encodings) can further enhance
 714 global awareness [Li et al. \(2020\)](#). Practical training relies on sampling and partitioning for
 715 scale [Chiang et al. \(2019\)](#); [Zheng et al. \(2020\)](#), with OGB benchmarks standardizing evaluation [Hu et al. \(2020\)](#).
 716

717 **Over-smoothing and over-squashing.** Deep stacks may over-smooth; curvature-inspired
 718 rewiring, residuals, and normalization layers are common responses. Over-squashing—the
 719 compression of exponentially many distant signals into fixed-size messages—can be alleviated by
 720 attention/edge weighting, graph rewiring, and subgraph-based encoders [Bronstein et al. \(2021\)](#).
 721

722 B.3 GENERATIVE FLOW NETWORKS (GFLOWNETS)

724 **Objective: sampling proportional to reward.** Given a set of terminal objects \mathcal{X} and a non-negative
 725 reward $R : \mathcal{X} \rightarrow \mathbb{R}_{\geq 0}$, GFlowNets seek a policy that samples $x \in \mathcal{X}$ with
 726

$$727 \quad P_\theta(x) \propto R(x), \quad P_\theta(x) = \sum_{\tau \in \mathcal{T}(x)} P_\theta(\tau), \quad (23)$$

728
 729

730 where $\tau = (s_0 \rightarrow \dots \rightarrow x)$ is a trajectory in a DAG of states and $\mathcal{T}(x)$ is the set of trajectories ending
 731 at x [Bengio et al. \(2021; 2023\)](#).
 732

733 **Detailed-balance (DB) and trajectory-balance (TB).** Let $F_\theta(s) > 0$ denote a learnable *flow*
 734 through state s . DB enforces local conservation:
 735

$$736 \quad F_\theta(s) P_\theta(s' | s) = F_\theta(s') P_\theta(s | s') \quad \text{for edges } s \leftrightarrow s'. \quad (24)$$

737

738 TB provides a path-wise condition linking forward/backward policies and a scalar Z_θ (partition
 739 function):
 740

$$740 \quad \mathcal{L}_{\text{TB}} = \mathbb{E}_\tau \left[(\log P_\theta(\tau) + \log Z_\theta - \log R(x))^2 \right], \quad (25)$$

741

742 encouraging $P_\theta(x) \propto R(x)$ when minimized [Malkin et al. \(2022\)](#). Subtrajectory balance (SubTB)
 743 generalizes TB to partial paths for credit assignment [Madan et al. \(2023\)](#).
 744

745 **Forward/backward policies and partition function.** A typical parameterization factors
 746 $P_\theta(\tau) = \prod_{t=0}^{T-1} P_\theta(s_{t+1} | s_t)$, $P_\theta(s_t | s_{t+1})$ learned for DB/SubTB, and treats Z_θ as a learnable
 747 scalar (or function) estimating $\sum_x R(x)$. Estimation stability can be improved via baselines,
 748 variance reduction, and regularization.
 749

750 **Mode coverage vs. RL/EBM/MCMC.** Unlike standard RL objectives that often favor a single
 751 high-return mode under sparse rewards, GFlowNets learn a distribution covering *multiple* modes.
 752 Compared to energy-based models (EBMs) and MCMC, GFlowNets amortize sampling via learned
 753 policies, reducing the need for long chains while retaining a reward-shaped target [LeCun et al.](#)
 754 (2006); [Salimans et al. \(2015\)](#); [Bengio et al. \(2023\)](#). Empirical applications span molecular design,
 755 program synthesis, and discrete structure generation [Zhang et al. \(2023\)](#); [Jain et al. \(2022\)](#), with
 ongoing work on offline training, replay buffers, and credit assignment [Lahlou et al. \(2023\)](#).

756 **C EXPERIMENT DETAILS**
757758 **C.1 METRIC DETAILS**
759

760 For all evaluation metrics, we provide definitions and brief interpretations. Let

761
$$\rho_d = \frac{\text{Cov}(\alpha(X_d), y_d)}{\sqrt{\text{Var}(\alpha(X_d)) \text{Var}(y_d)}} \quad (\text{cross-sectional correlation on day } d), \quad (26)$$

762
763

764 and let R_d denote the portfolio return constructed from α on day d , K the number of periods per
765 year (e.g., $K=252$ for daily), $r_{f,d}$ the risk-free rate, and

766
$$W_t = \sum_{u \leq t} (1 + R_u) \quad (\text{cumulative wealth}). \quad (27)$$

767
768

769

- **Information Coefficient (IC):** See Eq. 11. *Interpretation.* Cross-sectional predictive
770 power of the factor—how well $\alpha(X_d)$ aligns with next-period outcomes y_d . Using the
771 absolute value isolates *magnitude* rather than sign (long/short direction can be flipped).
772 Higher IC indicates more informative date-wise rankings and is a prerequisite for con-
773 structing profitable long–short portfolios.

774

- **Information Ratio of IC (ICIR):**

775
$$\text{ICIR} = \frac{\mathbb{E}_d[\rho_d]}{\sqrt{\text{Var}_d(\rho_d)}}. \quad (28)$$

776
777

778 *Interpretation.* Time-series consistency of cross-sectional predictability: mean IC relative
779 to its volatility. Under weak dependence, ICIR approximates a signal-to-noise measure
780 (akin to a t -statistic for $\mathbb{E}[\rho_d]$), favoring factors that work *consistently* rather than sporadi-
781 cally.782

- **Rank Information Coefficient (RankIC):**

783
$$\text{RankIC} = \left| \mathbb{E}_d[\rho_d^{\text{rank}}] \right|, \quad \rho_d^{\text{rank}} = \frac{\text{Cov}(\text{rank}(\alpha(X_d)), \text{rank}(y_d))}{\sqrt{\text{Var}(\text{rank}(\alpha(X_d))) \text{Var}(\text{rank}(y_d))}}. \quad (29)$$

784
785

786 *Interpretation.* Spearman-style counterpart to IC that evaluates whether higher-ranked sig-
787 nals correspond to higher-ranked outcomes. RankIC is robust to outliers and monotone
788 transforms of α , aligning with rank-based portfolio constructions.789

- **Information Ratio of RankIC (RankICIR):**

790
$$\text{RankICIR} = \frac{\mathbb{E}_d[\rho_d^{\text{rank}}]}{\sqrt{\text{Var}_d(\rho_d^{\text{rank}})}}. \quad (30)$$

791
792

793 *Interpretation.* Time-series stability of rank-based predictive power, prioritizing factors
794 whose cross-sectional ordering remains reliable across time.795

- **Annualized Return (AR):**

796
$$\text{AR} = K \cdot \mathbb{E}_d[R_d]. \quad (31)$$

797
798

799 *Interpretation.* Economic value produced by the portfolio rule induced by α . When com-
800 pounded is material, geometric annualization via W_t is preferred.801

- **Maximum Drawdown (MDD):**

802
$$\text{MDD} = -\max_t \left(1 - \frac{W_t}{\max_{u \leq t} W_u} \right). \quad (32)$$

803
804

805 *Interpretation.* Worst peak-to-trough loss of the wealth process; a trajectory- and tail-risk
806 metric not captured by variance alone. It is critical for leverage, risk limits, and investor
807 experience.808

- **Sharpe Ratio (SR) (annualized, excess over risk-free):**

809
$$\text{SR} = \frac{\sqrt{K} \mathbb{E}_d[R_d - r_{f,d}]}{\sqrt{\text{Var}_d(R_d - r_{f,d})}}. \quad (33)$$

810 *Interpretation.* Risk-adjusted return per unit of volatility for the α -induced portfolio, en-
811 abling fair comparison across methods, universes, and rebalancing frequencies.

810 **Reporting conventions.** (i) We report IC/RankIC in absolute value (cf. Eq. 11, Eq. 29) because
 811 factor signs are arbitrary up to inversion. (ii) For SR, we use excess returns $R_d - r_{f,d}$; To ensure
 812 fair comparison while simplifying the process, we set $r_{f,d}=0$ for comparability and state this choice
 813 explicitly. (iii) Due to differing rules between the CSI300/500 indices and the S&P500, when back-
 814 testing on the CSI300/500, we purchase the top 20% of stocks each trading day and sell them after
 815 20 days (long positions only); For the S&P500, we purchase the top 10% of stocks each trading day
 816 and sell them after 20 days, while simultaneously selling the bottom 10% of stocks and repurchasing
 817 them after 20 days (long-short combination).

818 C.2 HYPERPARAMETER SETTING

820 The hyperparameter settings of AlphaSAGE are listed in Table 3.

823 Table 3: The hyperparameter settings of AlphaSAGE.

Name	Description	Value
Max Length	The maximum number of tokens in the s_t	20
Hidden Dim	The dimension of hidden state	128
Encoder Layer	The number of layers in RGCN encoder	2
Entropy Coef	The weight of \mathcal{L}_{ENT}	0.01
Learning Rate	The learning rate to optimize θ	0.0001
SA Weight	The weight of R_{SA}	1.0
NOV Weight	The weight of R_{NOV}	0.3
Pool Capacity	The maximum number of alphas in alpha pool	50
Episodes	The number of trajectory sampling instances	10000/20000 ³

836 C.3 BASELINE DETAILS

837 We selected seven methods as the baseline:

- 840 • **MLP** [Murtagh \(1991\)](#): A feedforward neural network that maps tabular features to return
 841 targets, capturing nonlinear interactions. It is a strong generic baseline but can overfit
 842 without careful regularization and offers limited interpretability.
- 843 • **LightGBM** [Ke et al. \(2017\)](#): A gradient-boosted decision tree learner with histogram-based
 844 splits and leaf-wise growth, well suited to large, sparse, or heterogeneous financial features.
 845 It trains fast and handles missing values natively, though leaf-wise growth can overfit small
 846 samples without constraints.
- 847 • **XGBoost** [Chen & Guestrin \(2016\)](#): Boosted trees optimized with second-order information,
 848 shrinkage, column subsampling, and explicit regularization. Reliable on tabular alpha
 849 features, but the ensemble remains hard to interpret structurally and can be sensitive to label
 850 leakage or distribution shift.
- 851 • **GP** [Chen et al. \(2021\)](#): Genetic programming performs symbolic regression by evolving
 852 expression trees via mutation and crossover, yielding human-readable formulas. It explores
 853 large search spaces but is prone to bloat and may converge slowly under sparse, delayed
 854 rewards.
- 855 • **AlphaGen** [Yu et al. \(2023\)](#): Proposes mining *synergistic* sets of formulaic alphas by di-
 856 rectly optimizing the downstream combination model’s performance. Uses reinforcement
 857 learning to explore the expression search space, assigning the improvement in port-
 858 folio/combiner performance as the RL return so the generator preferentially discovers alphas
 859 that work well together.
- 860 • **AlphaQCM** [Zhu & Zhu \(2025\)](#): Frames synergistic alpha discovery as a non-stationary,
 861 reward-sparse MDP and adopts a *distributional* RL approach. Learns both a Q-function
 862 and quantiles, then applies a quantile conditional moment method to obtain an unbiased
 863 variance estimate; the learned value and variance jointly guide exploration under non-
 864 stationarity, improving search efficiency on large universes.

864

- **AlphaForge** Shi et al. (2025a): Introduces a two-stage framework that couples a generative–predictive neural module for factor proposal (encouraging broad, diverse exploration) with a dynamic combination stage. The combiner selects by recent performance and *adapts weights over time*, addressing inconsistency and rigidity of fixed-weight ensembles and yielding stronger portfolio results in empirical tests.

865

866

867

868

869

D IMPLEMENTATION DETAILS

D.1 PSEUDO CODE

870 The pseudo code of AlphaSAGE (core of mining framework) is shown in Algorithm 1. And the
 871 code is available at <https://anonymous.4open.science/r/AlphaSAGE-3BA9>.

Algorithm 1: AlphaSAGE

872 **Input:** Stock features X , stock trend labels y , action set \mathcal{A}
 873 **Output:** Final alpha pool \mathcal{F}

874 1 **Initialize:** GFN parameters θ ; probability buffer $\mathcal{B}_{\text{prob}} \leftarrow \emptyset$; embedding buffer $\mathcal{B}_{\text{emb}} \leftarrow \emptyset$; alpha
 875 pool $\mathcal{F} \leftarrow \emptyset$;

876 2 **for** $t = 1, 2, \dots, T_{\text{max}}$ **do**

877 3 Parse current state $s_t \rightarrow \text{ast}_t$;

878 4 Compute state embedding $e_t \leftarrow f_{\text{GNN}}(\text{ast}_t)$; // Eq. 7

879 5 Output action distribution $\pi_{\theta}(\cdot | \text{ast}_t)$; append to $\mathcal{B}_{\text{prob}}$;

880 6 **if** $\text{rand}() \geq p_{\text{es}}(s_t)$ **then**

881 $a_t \leftarrow \text{SEP}$;

882 **else**

883 $\text{Sample or select } a_t \in \mathcal{A} \text{ from } \pi_{\theta}(\cdot | \text{ast}_t)$;

884 7 **if** $a_t = \text{SEP}$ **then**

885 Build expression $\alpha \leftarrow \text{BuildExpr}(s_t)$;

886 Compute alpha $z \leftarrow \text{ComputeAlpha}(\alpha, X)$;

887 Compute correlation reward $R_{\text{IC}} \leftarrow \text{IC}(z, y)$; // Eq. 11

888 Compute novelty to pool members $R_{\text{NOV}} \leftarrow \text{Novelty}(z, \mathcal{F})$; // Eq. 12

889 Run KNN on terminal embedding e_t against pool embeddings:
 $\mathcal{N} \leftarrow \text{KNN}(e_t, \text{Emb}(\mathcal{F}), k)$;

890 8 Build distance-weight matrix $W \leftarrow \text{Dist2Weight}(\mathcal{N})$ and performance similarity
 $\text{sim} \leftarrow \text{PerfSim}(s, \mathcal{N}, W)$;

891 9 SA reward $R_{\text{SA}} \leftarrow \text{SAReward}(\text{sim})$; // Eq. 10

892 10 Total reward $R \leftarrow \text{Combine}(R_{\text{IC}}, R_{\text{NOV}}, R_{\text{SA}}, t)$; // Eq. 13

893 11 **if** $\text{PassThreshold}(R)$ **then**

894 12 $\mathcal{F} \leftarrow \mathcal{F} \cup \{\alpha\}$;

895 13 Append e_t to \mathcal{B}_{emb} ;

896 14 Trajectory Balance loss $\mathcal{L}_{\text{TB}} \leftarrow \text{TrajectoryBalance}(\mathcal{B}_{\text{prob}}, R)$; // Eq. 5

897 15 Entropy regularizer $\mathcal{L}_{\text{ent}} \leftarrow \text{EntropyReg}(\mathcal{B}_{\text{prob}})$; clear $\mathcal{B}_{\text{prob}}$;

898 16 Total loss $\mathcal{L}_{\text{final}} \leftarrow \mathcal{L}_{\text{TB}} + \lambda_{\text{ent}} \mathcal{L}_{\text{ent}}$; // Eq. 14

899 17 Update $\theta \leftarrow \theta - \eta \nabla_{\theta} \mathcal{L}_{\text{final}}$;

900 18 Reset $S_{t+1} \leftarrow \text{InitState}()$; clear $\mathcal{B}_{\text{prob}}$;

901 19 **else**

902 20 $\text{State transition } S_{t+1} \leftarrow \text{Transition}(S_t, a_t)$;

903 21 **return** \mathcal{F} ;

D.2 RELATION TYPE OF RGCN

913 To denote combinations between different operators and features, we have defined the following
 914 relationships: ① Unary operator with operand; ② Commutative operator with operands; ③
 915 Non-commutative operator with left operand; ④ Non-commutative operator with right operand; ⑤
 916 Rolling operator with feature operand; ⑥ Rolling operator with time operand.

918
 919 Table 4: Raw features and operators. **F**: base market features; **U/B**: unary/binary operators; **CS**:
 920 cross-sectional operation (within-day across assets); **TS**: time-series operation (rolling window).
 921 The lookback length d denotes the past d trading days, and the ϵ is used only for numerical stability.

Name	Type	Description
Open	F	Opening price
Close	F	Closing price
High	F	Daily highest price
Low	F	Daily lowest price
Vwap	F	Daily average price, weighted by the volume of trades at each price
Volume	F	Trading volume (number of shares)
Abs	U	Absolute value of the input
Slog1p	U	Signed log transform: sign(input) times log of (1 plus the absolute value)
Inv	U	Reciprocal of the input; add ϵ to avoid division by zero
Sign	U	Sign of the input, returning -1, 0, or 1
Log	U	Natural logarithm of the input; add ϵ for numerical stability
Rank	U-CS	Cross-sectional rank normalization within a day, mapped to the range [0, 1]
Add	B	Element-wise addition of two inputs
Sub	B	Element-wise subtraction: first minus second
Mul	B	Element-wise multiplication
Div	B	Element-wise division; add a small constant to the denominator for stability
Pow	B	Element-wise power: raise the first input to the power of the second
Greater	B	Element-wise comparison: 1 if first input is greater than second, else 0
Less	B	Element-wise comparison: 1 if first input is less than second, else 0
Ref	U-TS	Lag operator: the value from d days ago
TsMean	U-TS	Rolling mean over the past d days
TsSum	U-TS	Rolling sum over the past d days
TsStd	U-TS	Rolling standard deviation over the past d days
TsIr	U-TS	Rolling information ratio over the past d days
TsMinMaxDiff	U-TS	Rolling range over the past d days (rolling max minus rolling min)
TsMaxDiff	U-TS	Current value minus the rolling max over the past d days
TsMinDiff	U-TS	Current value minus the rolling min over the past d days
TsVar	U-TS	Rolling variance over the past d days
TsSkew	U-TS	Rolling skewness over the past d days
TsKurt	U-TS	Rolling kurtosis over the past d days
TsMax	U-TS	Rolling maximum over the past d days
TsMin	U-TS	Rolling minimum over the past d days
TsMed	U-TS	Rolling median over the past d days
TsMad	U-TS	Rolling median absolute deviation over the past d days
TsRank	U-TS	Rolling rank of the current value within the past d days, mapped to [0, 1]
TsDelta	U-TS	Change over d days: current value minus the value d days ago
TsDiv	U-TS	Ratio over d days: current value divided by the value d days ago
TsPctChange	U-TS	Percentage change over the past d days
TsWMA	U-TS	Linearly decaying weighted moving average over the past d days
TsEMA	U-TS	Exponential moving average with a decay over the past d days
TsCov	B-TS	Rolling covariance between two inputs over the past d days
TsCorr	B-TS	Rolling Pearson correlation between two inputs over the past d days

D.3 FEATURES AND OPERATORS

967
 968 All operators and features available during alpha mining are listed in the Table 4.
 969
 970

972 **E PROOF**
 973

974 **Proposition E.1** (Alpha Diversity Stabilizes Estimation and Prediction). *Let $F = [\alpha_1, \dots, \alpha_N] \in$
 975 $\mathbb{R}^{T \times N}$ collect N standardized alphas (each column has mean 0 and variance 1), and let $y \in \mathbb{R}^T$ be
 976 the target return. Define*

977
$$\Sigma = \frac{1}{T} F^\top F \in \mathbb{R}^{N \times N}, \quad g = \frac{1}{T} F^\top y \in \mathbb{R}^N. \quad (34)$$

 978

980 *The OLS estimator is $\hat{\beta} = \Sigma^{-1}g$. Suppose $\epsilon = y - F\beta^*$ satisfies $\mathbb{E}[\epsilon] = 0$ and $\text{Var}(\epsilon) = \sigma^2 I_T$.
 981 Then:*

982 1. *(Estimator variance decomposition) Writing the eigendecomposition $\Sigma = Q\Lambda Q^\top$ with
 983 eigenvalues $1 \geq \lambda_1 \geq \dots \geq \lambda_N > 0$, we have*

985
$$\text{Var}(\hat{\beta}) = \frac{\sigma^2}{T} \Sigma^{-1} \Rightarrow \text{tr} \text{Var}(\hat{\beta}) = \frac{\sigma^2}{T} \sum_{i=1}^N \frac{1}{\lambda_i}. \quad (35)$$

 986

988 *Consequently, as pairwise correlations increase and the spectrum becomes more ill-
 989 conditioned (small λ_{\min}), the total estimation variance inflates.*

990 2. *(Prediction risk amplification) The in-sample prediction variance satisfies*

992
$$\mathbb{E}[\|F(\hat{\beta} - \beta^*)\|_2^2] = \text{tr}(F \text{Var}(\hat{\beta}) F^\top) = \frac{\sigma^2}{T} \text{tr}(F \Sigma^{-1} F^\top) = \sigma^2 \text{tr}(\Sigma \Sigma^{-1}) = \sigma^2 N, \quad (36)$$

 993

995 *but the out-of-sample risk for a new design with the same second moments equals*

996
$$\mathcal{R}_{\text{pred}} = \sigma^2 + \mathbb{E}[(\alpha^\top(\hat{\beta} - \beta^*))^2] = \sigma^2 + \frac{\sigma^2}{T} \text{tr}(\Sigma \Sigma^{-1}) = \sigma^2 \left(1 + \frac{N}{T}\right), \quad (37)$$

 997

999 *while the uncertainty allocation across coordinates is governed by Σ^{-1} : higher multi-
 1000 collinearity (smaller λ_{\min}) yields larger coordinate-wise dispersion of $\hat{\beta}$ and hence less
 1001 interpretability.*

1002 3. *(Sensitivity to perturbations) For perturbations $(\Delta\Sigma, \Delta g)$, the linear system $\Sigma\hat{\beta} = g$ obeys
 1003 the classical bound*

1004
$$\frac{\|\Delta\hat{\beta}\|_2}{\|\hat{\beta}\|_2} \lesssim \kappa_2(\Sigma) \left(\frac{\|\Delta g\|_2}{\|g\|_2} + \frac{\|\Delta\Sigma\|_2}{\|\Sigma\|_2} \right), \quad (38)$$

 1005

1006 *where $\kappa_2(\Sigma) = \|\Sigma\|_2 \|\Sigma^{-1}\|_2 = \lambda_{\max}/\lambda_{\min}$. Thus, near-collinearity (large κ_2) makes $\hat{\beta}$
 1007 highly unstable under small data noise or distributional drift.*

1008 4. *(Two-alpha closed form) For two standardized alphas with correlation ρ ,*

1009
$$\Sigma = \begin{bmatrix} 1 & \rho \\ \rho & 1 \end{bmatrix}, \quad \Sigma^{-1} = \frac{1}{1-\rho^2} \begin{bmatrix} 1 & -\rho \\ -\rho & 1 \end{bmatrix}, \quad (39)$$

 1010

1011 *so $\text{Var}(\hat{\beta}) = \frac{\sigma^2}{T(1-\rho^2)} \begin{bmatrix} 1 & -\rho \\ -\rho & 1 \end{bmatrix}$ and $\kappa_2(\Sigma) = \frac{1+\rho}{1-\rho}$. As $\rho \rightarrow 1$, both the variance and the
 1012 condition number blow up.*

1013 5. *(Equicorrelated family) If Σ has equicorrelation ρ off-diagonal, then*

1014
$$\lambda_1 = 1 + (N-1)\rho, \quad \lambda_2 = \dots = \lambda_N = 1 - \rho, \quad (40)$$

 1015

1016 *and hence*

1017
$$\text{tr} \text{Var}(\hat{\beta}) = \frac{\sigma^2}{T} \left(\frac{1}{1 + (N-1)\rho} + \frac{N-1}{1-\rho} \right), \quad \kappa_2(\Sigma) = \frac{1 + (N-1)\rho}{1-\rho}. \quad (41)$$

 1018

1019 *Even modest $\rho > 0$ causes variance inflation linear in N through the $(N-1)/(1-\rho)$
 1020 term; promoting diversity (smaller ρ) sharply reduces this inflation.*

1026 *Proof.* (1) Since $\hat{\beta} = (F^\top F)^{-1} F^\top y = \Sigma^{-1} g$ and $y = F\beta^* + \epsilon$ with $\text{Var}(\epsilon) = \sigma^2 I_T$, we have
 1027

$$1028 \text{Var}(\hat{\beta}) = \Sigma^{-1} \left(\frac{1}{T^2} F^\top \text{Var}(y) F \right) \Sigma^{-1} = \Sigma^{-1} \left(\frac{\sigma^2}{T^2} F^\top F \right) \Sigma^{-1} = \frac{\sigma^2}{T} \Sigma^{-1}. \quad (42)$$

1031 Using $\Sigma = Q\Lambda Q^\top$ yields $\text{tr} \text{Var}(\hat{\beta}) = \frac{\sigma^2}{T} \sum_i \lambda_i^{-1}$.
 1032

1033 (2) For in-sample variance,

$$1034 \mathbb{E} \|F(\hat{\beta} - \beta^*)\|_2^2 = \text{tr}(F \text{Var}(\hat{\beta}) F^\top) = \frac{\sigma^2}{T} \text{tr}(F \Sigma^{-1} F^\top). \quad (43)$$

1037 Since $F \Sigma^{-1} F^\top$ and $\Sigma \Sigma^{-1}$ share the same trace ($\text{tr}(AB) = \text{tr}(BA)$), this equals $\sigma^2 \text{tr}(I_N) = \sigma^2 N$. For a new draw $\tilde{\alpha}$ with the same second moments, $\mathbb{E}[\tilde{\alpha} \tilde{\alpha}^\top] = \Sigma$, so the added generalization
 1038 variance is $\frac{\sigma^2}{T} \text{tr}(\Sigma \Sigma^{-1}) = \frac{\sigma^2 N}{T}$, giving $\mathcal{R}_{\text{pred}} = \sigma^2(1 + N/T)$; however the *distribution* of this
 1039 uncertainty over coordinates is governed by Σ^{-1} , worsening with ill-conditioning, which harms
 1040 interpretability of individual $\hat{\beta}_i$.
 1041

1042 (3) The stated perturbation bound follows from standard linear system sensitivity: for $\Sigma \hat{\beta} = g$, first-order analysis (or the Bauer–Fike–type arguments) gives $\|\Delta \hat{\beta}\|_2 \lesssim \|\Sigma^{-1}\|_2 (\|\Delta g\|_2 + \|\Delta \Sigma\|_2 \|\hat{\beta}\|_2)$; normalizing by $\|\hat{\beta}\|_2$ and noting $\|\Sigma^{-1}\|_2 \|\Sigma\|_2 = \kappa_2(\Sigma)$ yields the claim.
 1043

1044 (4)–(5) The two-alpha and equicorrelation calculations follow from direct inversion and the known
 1045 eigenstructure: for equicorrelation, the all-ones vector is the top eigenvector with eigenvalue $1 + (N - 1)\rho$ and the orthogonal complement has eigenvalue $1 - \rho$. Plugging these into part (1) gives
 1046 the trace formula and condition number.
 1047

1048 Collectively, (1)–(5) show that reducing off-diagonal correlations increases the eigenvalues of Σ , de-
 1049 creases $\kappa_2(\Sigma)$, shrinks $\text{Var}(\hat{\beta})$, and improves stability and interpretability—formally substantiating
 1050 the need for diverse, weakly correlated alphas. \square
 1051

1052 **Corollary E.2** (Regularization as a proxy for diversity). *For ridge with penalty $\lambda > 0$, $\hat{\beta}_\lambda =$*
 1053 $(\Sigma + \lambda I)^{-1} g$ and

$$1054 \text{Var}(\hat{\beta}_\lambda) = \frac{\sigma^2}{T} (\Sigma + \lambda I)^{-1} \Rightarrow \text{tr} \text{Var}(\hat{\beta}_\lambda) = \frac{\sigma^2}{T} \sum_{i=1}^N \frac{1}{\lambda_i + \lambda}. \quad (44)$$

1055 Either increasing diversity (raising the λ_i) or increasing λ reduces variance; explicit diversity control
 1056 targets the spectrum directly, often achieving lower variance without the shrinkage bias inherent
 1057 in ridge.
 1058

1064 F ADDITIONAL RESULTS

1066 F.1 BACKTESTING RESULTS

1067 Figure 5 shows that on **CSI500** (2022–2024) AlphaSAGE delivers the strongest end-period wealth
 1068 and sustains a clear lead for most of the horizon. It experiences *smoother drawdowns* around mid-
 1069 2023, *recovers earlier* from late-2024 stress, and *retains* more of the subsequent rally; all baselines
 1070 trail, while the CSI500 index lags markedly throughout.
 1071

1072 Figure 6 shows that on **S&P500** (2018–2021) AlphaSAGE tracks near the top during calm phases,
 1073 then *recovers faster* and *compounds higher* after the 2020 drawdown, finishing with the best cu-
 1074 mulative return. Several baselines (e.g., AlphaForge) are competitive early but fail to match the
 1075 late-period acceleration; the market index remains below AlphaSAGE by the end.
 1076

1077 F.2 PARAMETER ANALYSIS

1078 This appendix reports two practical knobs: *training steps* and *candidate-pool size*. We track corre-
 1079 lation metrics (IC/RIC, ICIR/RICIR) and portfolio metrics (AR, MDD, SR).

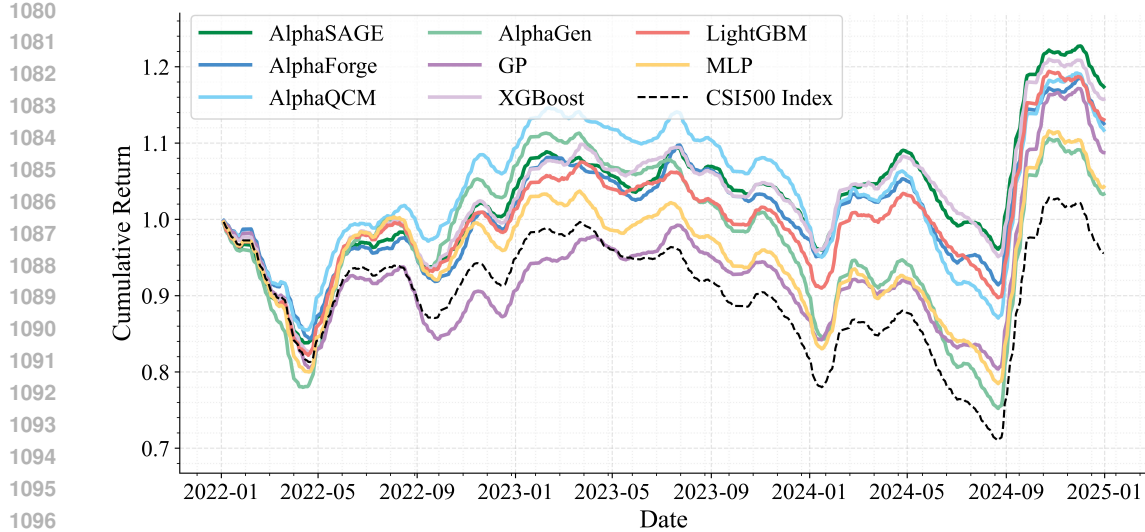


Figure 5: Cumulative return on CSI500 (2022–2024). Comparison among AlphaSAGE (ours), all baselines, and CSI500 Index benchmark.

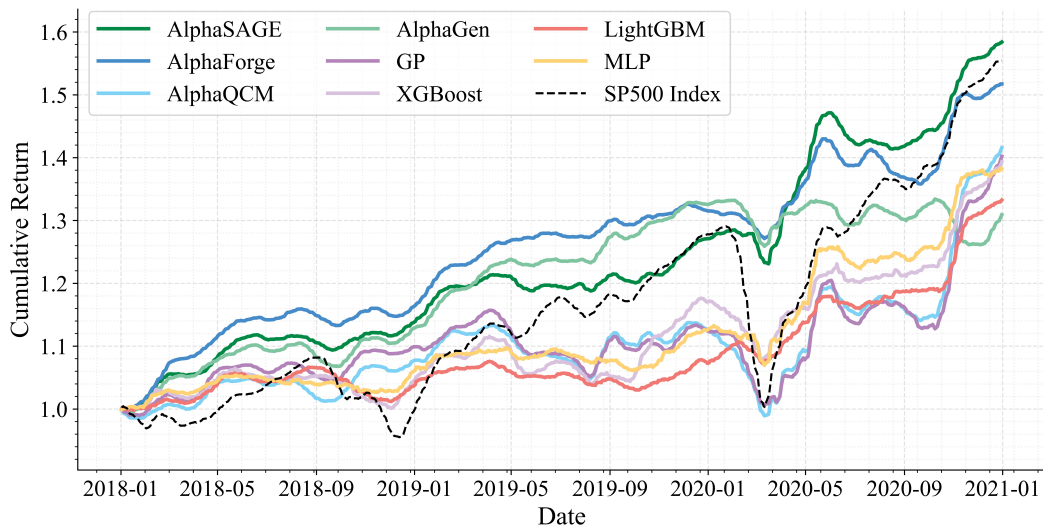


Figure 6: Cumulative return on S&P500 (2018–2020). Comparison among AlphaSAGE (ours), all baselines, and S&P500 Index benchmark.

Training steps. As shown in Fig. 7, **GFlowNets converge faster and train more efficiently than PPO** in the alpha-mining setting. IC/RIC and ICIR/RICIR rise sharply in early iterations and reach a high, stable plateau with lower variance; PPO improves more slowly and exhibits larger oscillations throughout.

Candidate-pool size. Figure 8 shows that **increasing the factor pool yields rapid gains followed by saturation**. All correlation metrics (IC/RIC, ICIR/RICIR) and portfolio metrics (AR, SR) improve markedly when moving from very small to moderate pool sizes, then flatten into broad plateaus; MDD improves monotonically with no instability.

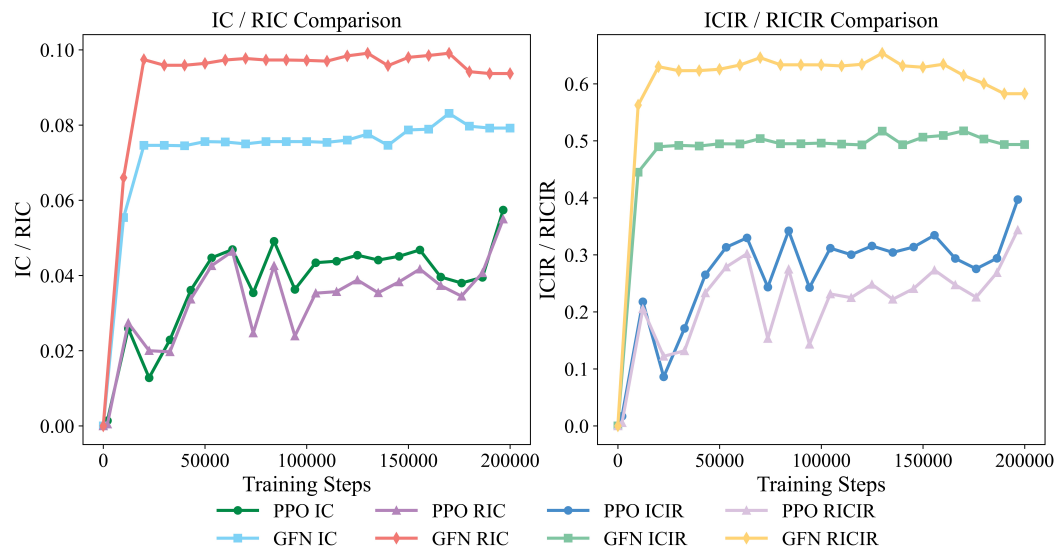


Figure 7: **Learning dynamics vs. training steps.** GFlowNets (GFN) achieve higher plateaus earlier and with less volatility than PPO across IC/RIC and ICIR/RICIR.

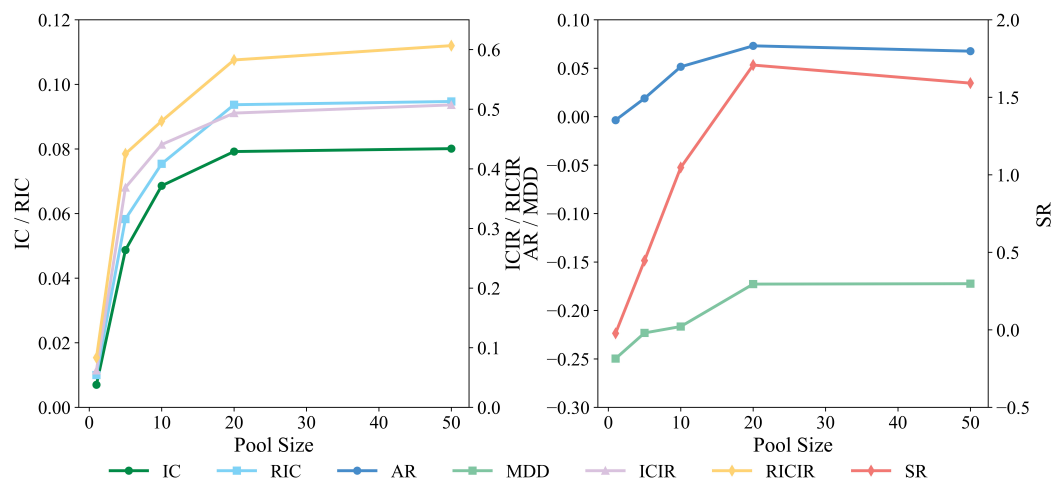


Figure 8: **Effect of candidate-pool size.** Metrics increase quickly at small–moderate pool sizes and then stabilize, indicating diminishing returns beyond a modest pool.